Materials Horizons

Volume 5
Number 3
May 2018
Pages 311-580

rsc.li/materials-horizons

ISSN 2051-6347

ROYAL SOCIETY OF CHEMISTRY

COMMUNICATION
Blaise L. Tardy, Orlando J. Rojas et al
Biofabrication of multifunctional nanocellulosic 3D structures:
a facile and customizable route

ROYAL SOCIETY OF CHEMISTRY

rsc.li/materials-horizons

Catalytic Reduction of Nitrogen to Produce Ammonia by Bismuth-based Catalysts: State of the Art and Future Prospects

Qiang Hao,[a] Chuangwei Liu,[b] Guohua Jia,[c] Yuan Wang,[d] Hamidreza Arandiyan,[e] Wei Wei,[a]

Bing-Jie Ni[a]*

[a] *Centre for Technology in Water and Wastewater (CTWW), School of Civil and Environmental Engineering, University of Technology Sydney (UTS), Sydney, NSW 2007, Australia*

[b] *Department of Energy Conversion and Storage, Technical University of Denmark，Lyngby, 2800, Denmark*

[c] *Curtin Institute of Functional Molecules and Interfaces, School of Molecular and Life Sciences, Curtin University, WA, 6845, Australia*

[d] *School of Chemistry, Faculty of Science, The University of New South Wales, Sydney, New South Wales 2052, Australia*

[e] *Laboratory of Advanced Catalysis for Sustainability, School of Chemistry, The University of Sydney, Sydney 2006, Australia*

ORCID:

Qiang Hao: 0000-0001-9981-7499   Chuangwei Liu: 0000-0002-8256-6053

Guohua Jia: 0000-0003-1179-2763   Bing-Jie Ni: 0000-0002-1129-7837

Yuang Wang: 0000-0002-5215-0487   Hamidreza Arandiyan: 0000-0001-5633-3945

*Corresponding author:

Prof. Bing-Jie Ni

Tel.: +61 295147401

E-mail: bingjieni@gmail.com

TOC
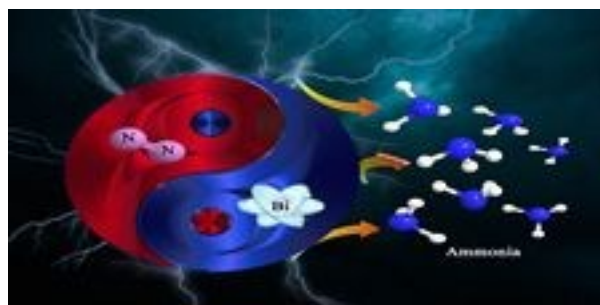
This review provides an up-to-date review on Bi-based nitrogen-fixation materials and future directions of the developments of new Bi-based nitrogen-fixation materials under ambient condition.

Materials Horizons Accepted Manuscript

Abstract

Ammonia is a key industrial raw material for fertilisers, chemicals and energy. The annual artificial ammonia synthesis via the Haber-Bosch process causes about 2% of global energy consumption and can lead to 1.6% CO_2 emission. It is urgent to develop low-cost and environmentally friendly approaches for artificial ammonia synthesis under ambient condition. Recently, bismuth (Bi)-based catalysts have attracted great interests due to their excellent nitrogen fixation performance in electrochemical and photocatalytic fields. However, there is still a lack of comprehensive review on Bi-based nitrogen-fixation materials focusing on the crystal structure, surface engineering and modification methods, which is highly desired for facilitating its further development towards applications. Herein, we provided an up-to-date review on Bi-based nitrogen-fixation materials and classified them as metallic Bi, bismuth oxide, bismuth oxyhalide, and Bi-based polyoxometalates. Starting from the underlying crystal structure, we analysed the internal electric field, surface engineering and modification methods of Bi-based nitrogen fixation materials. Then, we highlighted the latest achievements of Bi-based materials and revealed the challenges and obstacles in the development and application of Bi-based nitrogen-fixation materials. More importantly, this review presented the surface and structure engineering strategies, and future directions of the developments of new Bi-based nitrogen-fixation materials under ambient condition.

1. Introduction

Ammonia is an important industrial raw material that is widely used in the production of fertilisers, refrigerants and other chemicals. Every year, 750,000 tons of ammonia is produced and 88% of which are used as fertilisers.[1-3] Due to its high energy density (17.8 wt% hydrogen content) and zero carbon emissions, ammonia molecules are also potential energy storage and distribution media, providing the optimised solution for the energy crisis.[4] Nowadays, the commercial ammonia is primarily produced by the Haber-Bosch process, which uses the iron-based catalysts that require nitrogen (N_2), hydrogen (H_2), high pressure (15–25 MPa) and high temperature (400–500 °C).[5, 6] As a result, the leading industrial procedure for ammonia production accounts for about 2% of total energy consumption and can lead to 1.6% CO_2 emission per year.[7]

In contrast, artificial ammonia synthesis under ambient condition can reduce fossil fuel consumption and greenhouse gas emissions that contribute to global warming. Thus, the development of low-cost and environmentally friendly methods of photochemical or electrochemical N_2 fixation has crucial potential. There are increasing studies that have devoted to this topic recently and more than 450 papers in this area have been published in the last 5 years. These emerging researches aimed to fundamentally change the traditional ammonia synthesis, which does not require high energy consumption, high pressure or dangerous gas resources. The process only consumes a small amount of electrical energy or just free solar energy.[8-10]

However, there is still a huge gap between fundamental research and industrial

application, because of the low ammonia yield rate in artificial ammonia synthesis. Therefore, it is a crucial issue for the synthesis of highly efficient N_2-fixation materials and developing effective approaches to improve their performance. As active materials for photo/electrocatalytic ammonia synthesis, bismuth (Bi)-based materials including metallic bismuth, bismuth oxide, bismuth oxyhalide, and bismuth molybdate have been extensively studied particularly due to their advantages of being non-carcinogenic and non-toxic as well as their excellent catalytic properties in many fields.[11-13] Compared with common photocatalysts (TiO_2, g-C_3N_4 etc) and electrocatalysts (porous C-N, Pt/C etc), Bi-based showed significantly higher performance, which is caused by its strong chemical interaction with N_2 molecules (**Table 1**).[12] The previous reviews simply summarised the materials which can be used as photocatalyst or electrocatalysts in general, however a comprehensive review of Bi-based nitrogen-fixation materials towards emerging applications is still lacking,[14-16] which is of significance for facilitating its further development towards application.

Herein, we provided an up-to-date review on Bi-based nitrogen-fixation materials comprehensively, in which we classified the bismuth-based nitrogen-fixation materials as metallic Bi, bismuth oxide, bismuth oxyhalide, and Bi-based polyoxometalates. Starting from the underlying crystal structure, we firstly analysed the internal electric field, surface engineering and modification method of Bi-based nitrogen fixation materials. We then highlighted the latest achievements of Bi-based materials and revealed the challenges and obstacles in the development and application of Bi-based nitrogen-fixation materials. Finally, we also presented the strategies and future

directions of the developments of new Bi-based nitrogen-fixation materials under

ambient condition.

Table 1: Comparation of the catalytic performance of Bi-based materials and other typical

materials

Catalyst	Type	NH$_3$ yield	Reference
TiO$_2$	Photocatalysis	4.17 μmol/g/h	17
Fe-doped TiO$_2$	Photocatalysis	400 μmol/g/h	18
g-C$_3$N$_4$	Photocatalysis	141.7 μmol/g/h	19
Pt-CdS	Photocatalysis	16.3 μmol/g/h	20
Bi$_2$MoO$_6$	**Photocatalysis**	**1300 μmol/g/h**	**21**
BiOBr	**Photocatalysis**	**223.3 μmol/g/h**	**22**
BiO	**Photocatalysis**	**1226 μmol/g/h**	**12**
Ru/Ti	Electrocatalysis	7.78 μg/cm^2/h	23
Pt/C	Electrocatalysis	4.5 μg/cm^2/h	24
Porous C-N	Electrocatalysis	15.7 μg/cm^2/h	25
Bi$_4$V$_2$O$_{11}$/CeO$_2$	**Electrocatalysis**	**23.21 μg/cm^2/h**	**26**
Bi	**Electrocatalysis**	**936 μg/cm^2/h**	**27**

## 2. Catalytic N$_2$ fixation processes and limits

2.1 Adsorption and activation of N$_2$

The adsorption and activation of N$_2$ are generally considered to be the rate-

determining step of N$_2$ fixation. Since the N$_2$ molecules are stable and the coordination

is low, it is challenging to form chemical adsorption on the surface of the catalysts,

which dramatically limits the N_2-fixation efficiency. As shown in **Fig. 1a**, there are five

valence electrons in the $2s$ and $2p$ orbitals in a N atom, three of which are unpaired.

After bonding, the hybridisation of the atomic orbitals is separated into four bonding

orbitals (two σ orbitals and two π orbitals) and four anti-bonding orbitals (two σ*

orbitals and two π* orbitals). The gap between the lowest unoccupied molecular orbital

and the highest occupied molecular orbital is 10.82 eV, and it has a high ionisation

energy of 15.58 eV.[28] Therefore, the N≡N has very high bond energy, making it difficult

to directly cleave the triple bond as this step requires an energy of 945 kJ/mol.[29] Inspired

by natural nitrogenase, several transition-metal (based on Fe, Mo or V elements)

catalysts have been developed for N_2 fixation under ambient condition. There is a strong

interaction between the metals and the N $2p$ states, which can make N_2 molecules

chemically adsorbed on the surface of catalysts. Compared with physical adsorption,

chemical adsorption is much stronger. More importantly, the interaction provides a

pathway for the electrons to transfer from the catalysts to N_2, which can effectively

promote the activation of N_2 molecules.

After adsorption, electrons from the catalysts can be donated to the antibonding

π* orbitals of N_2, increasing the N≡N bond length and weakening its bond energy,

which is distinctive for the cleavage of N_2. For example, the N≡N bond has an original

length of 1.078 Å, and by obtaining electrons from BiOBr photocatalyst (an elementary

step for converting N_2 to N_2H* species), its length can be stretched to 1.133 Å (**Fig. 1b,**

c).[22]

Materials Horizons Accepted Manuscript
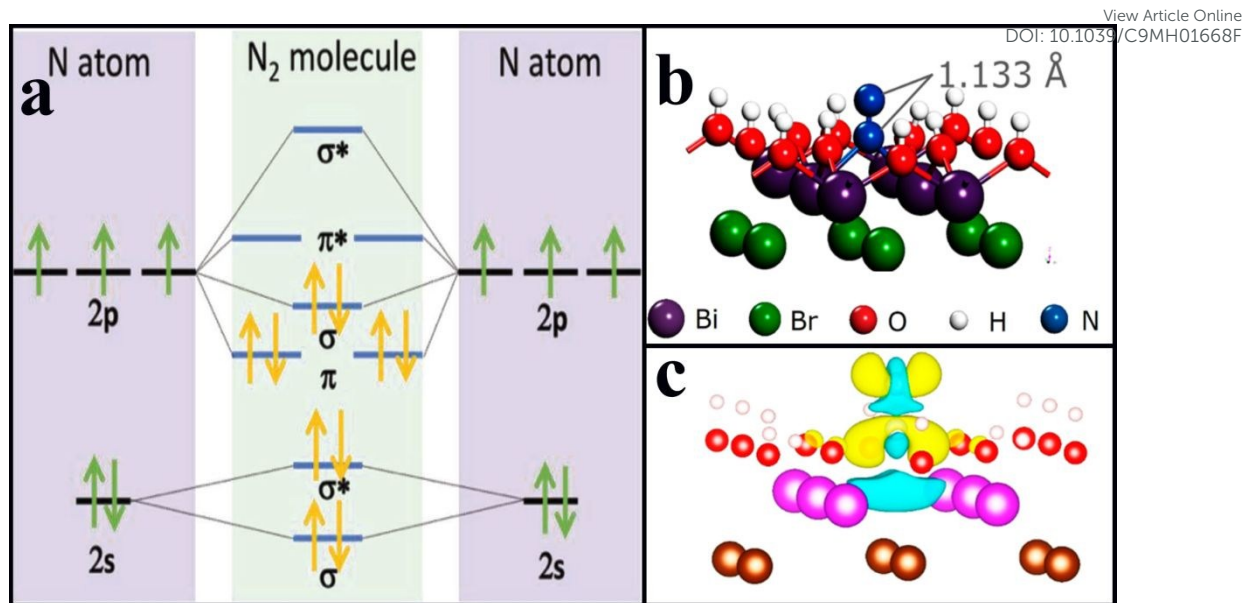
Fig. 1 (a) The diagrams of N atomic orbitals and their hybridisation of N_2 molecular orbitals. Reproduced with permission.[14] Copyright 2018, Wiley-VCH. (b) The adsorption geometry of N_2 on the oxygen vacancies of BiOBr (001) surface. (c) The charge density difference of the N_2-adsorbed (001) surface. The yellow and blue isosurfaces represent charge accumulation and depletion in the space, respectively. (b, c) Reproduced with permission.[22] Copyright 2015, American Chemical Society.

2.2 Pathway of N_2 fixation

The investigation of the catalytic N_2-fixation pathway is crucial for studying the reaction mechanism, which is a conducive issue for the realisation of artificial N_2 fixation. At present, there are two mechanisms and three pathways recognised in the field, including the associative mechanism and the dissociative mechanism.[30-32] In the dissociative mechanism, the N≡N bonds of adsorbed N_2 molecules should be broken before the hydrogenation reaction. Then the formed two individual N atoms on the surface of catalysts will take part in further reactions to form ammonia respectively (**Fig. 2a**). The dissociative mechanism has been confirmed to be what occurs during the Haber-Bosch process. However, the cleavage of N≡N bonds requires a large amount of energy. Thus the dissociative mechanism may not be common in catalytic N_2 fixation

under ambient condition.[30] On the contrary, when the molecule is hydrogenated in the associative mechanism, two nitrogen centres in N_2 remain bound to each other until the last N-N bond breaks, and NH_3 can be released. The following are two possible pathways of associative mechanism: on the one hand, hydrogenation may occur preferentially on the nitrogen furthest from the catalyst, resulting in the release of one equivalent of NH_3 and leaving the metal nitrido until hydrogenation yields the last equivalent of NH_3 (**Fig. 2b**); on the other hand, the second type of associative mechanism calls for that each of the two nitrogen centres undergo a single hydrogenation events in sequence until one of the nitrogens is converted to NH_3 and the N-N bond is broken (**Fig. 2c**).[15] The associative mechanisms are more likely to occur in electrochemical or photocatalytic N_2 fixation.
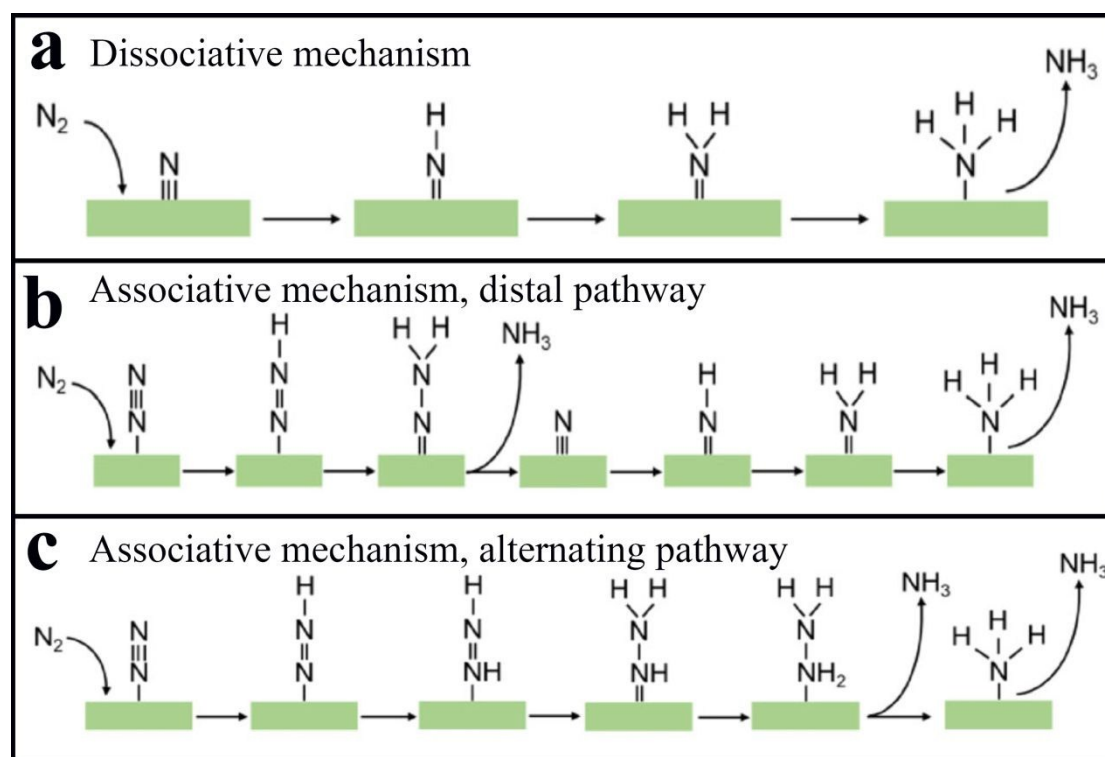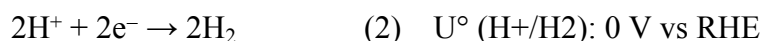

Fig. 2 The possible N_2-fixation pathways on the surface of catalysts. (a) The dissociative mechanism and (b, c) the associative mechanisms. (a-c) Reproduced with permission.[16] Copyright 2019, Nature-Springer.

Materials Horizons Accepted Manuscript

2.3 Limits of artificial N_2 fixation

The catalytic reaction system for synthesising ammonia usually consists of the catalysts and water, and there are a few key factors that limit the yield of ammonia. Firstly, the low solubility of N_2 in aqueous solution (20 mg/L, 20 °C, 100 kPa) greatly limits the contact area and time between the catalysts and the N_2 in the water, thereby limiting the rate of N_2 fixation (**Fig. 3a**). Secondly, it is very difficult for N_2 molecules to be strongly adsorbed and activated on the surface of catalysts, as it has stable chemical properties (**Fig. 3b**). Thirdly, the competitive hydrogen evolution reaction (HER) can rip electrons, reducing the selectivity of N_2 fixation. Oshikiri el al. reported an Au nanoparticle modified $SrTiO_3$ photoelectrode for N_2 fixation under visible light irradiation.[33] In this system, the following two reactions proceed:

$$N_2 + 6H^+ + 6e^- \rightarrow 2HN_3 \quad (1) \quad U° (N2/NH3): \text{-}0.092 \text{ V vs RHE}$$

$$2H^+ + 2e^- \rightarrow 2H_2 \quad\quad\quad (2) \quad U° (H+/H2): 0 \text{ V vs RHE}$$

As the standard redox potential of N_2 reduction is more negative than that of HER, the competitive HER is a significant barrier for N_2 reduction (**Fig. 3c**). While Bi-based catalysts have many advantages (i.e., unique structure to capture and activate N_2, low adsorption energy of H_2, etc.) in solving these limiting factors, the Bi-based catalysts may form a unique and effective platform in N_2-reduction area.
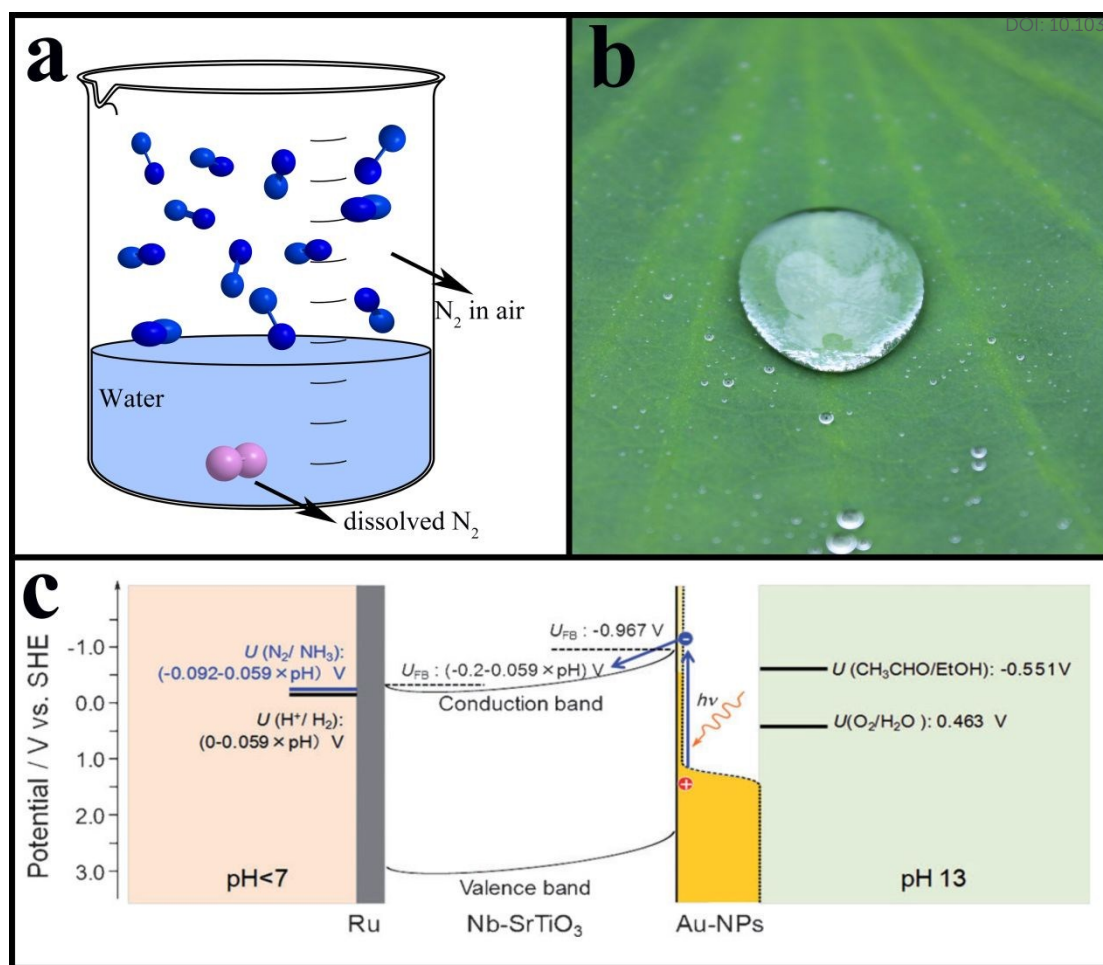
Fig. 3 (a) Schematic of dissolved N_2 in water; (b) diagram of N_2 on the clean surface of catalysts which is being analogous to water on the surface of hydrophobic lotus leaf; (c) an energy diagram of the plasmon-induced ammonia photosynthesis system using a $SrTiO_3$ substrate loaded with Au nanoparticles. (c) Reproduced with permission.[33] Copyright 2014, Wiley-VCH.

3. Structure and functionalization of Bi-based materials

3.1 Metallic Bi

The atomic number of Bi in the periodic table of elements is 83.[34] Unlike its ortho-elements, the 82nd of lead and 84th elements of polonium which are toxic, Bi is a non-toxic heavy metallic element. The crystal structure of Bi **Fig. 4a** shows that it belongs to the trigonal crystal system (a = b = 4.53 Å, c = 11.81 Å) and R3m (166) space group.[35]

Bulk metallic Bi is a semimetal with direct plasmonic effect.[36] For the advances of long Fermi wavelength, high carrier motilies and surface plasmon resonance (SPR) effect, it has attracted a lot of research interests, especially in the field of photocatalysis and electrocatalysis.[37-40] Due to the quantum confinement phenomena and low energy overlap of Bi, it can be converted to semiconductor from semimetal when it becomes thin films.[41, 42] Very recently, researchers found that metallic Bi can be used in electrocatalytic N_2 reduction.[11, 27] The semiconducting Bi is less-reactive in HER reaction because of the high free energy barrier of adsorption between Bi and H_2.[43] The strong interaction between the Bi $6p$ band the N $2p$ orbitals allows N_2 to be selectively adsorbed on its surface, which contributes to the dissociation of N≡N.[27] Besides, Bi atoms in Bi-based catalysts can localize the density state near its Fermi level, which means that Bi atoms can provide more active centres for activating N_2 by donating p-electrons.[12] At the same time, Bi is able to reduce the free-energy change in the potential-determining step.[27] The above facts are all favourable for the N_2 reduction reaction. Furthermore, Hao et al. found that Bi and potassium cations (K^+) pairs can ulteriorly reduce the reactional free-energy change, adjust the proton diffusion process, stabilise intermediates of N_2 reduction and boost the N_2 fixation efficiency.[27] It has been confirmed that two-dimensional Bi nanosheets with ample edge sites and delocalised p-orbital electrons show excellent electrocatalytic performance of N_2 fixation.[11] It has also been found that surface defects can influence the N_2 fixation performance of metallic Bi. Wang et al. prepared Bi nanoplates by the reduction of Bi_2O_3 (**Fig. 4b**). As shown in the Gibbs-free-energy diagrams (**Fig. 4c**), the ΔG_{N2H}* defective Bi (110) is

much lower than that of ideal Bi (110). The volcano plot of the potential-limiting steps

and ΔG_{N2H*} were exhibited in **Fig. 4d**. The Gibbs free energy of N₂H* on defective Bi

(110) is 0.89 eV, which is closer to the peak than other metals such as Pt, Pd, and Cu.

The HER performances of different catalysts listed in **Fig. 4e** demonstrates the

hydrogen-generation activity of Bi is poor, due to its low adsorption energy of H. The

activation energy of N_2 of the ideal Bi (110) is 1.03 eV, while it can be reduced to 0.56

eV on the surface of defective Bi (110) (**Fig. 4f**), indicating that N_2 can be more easily

and dynamically fixated on defective Bi (110).[44]
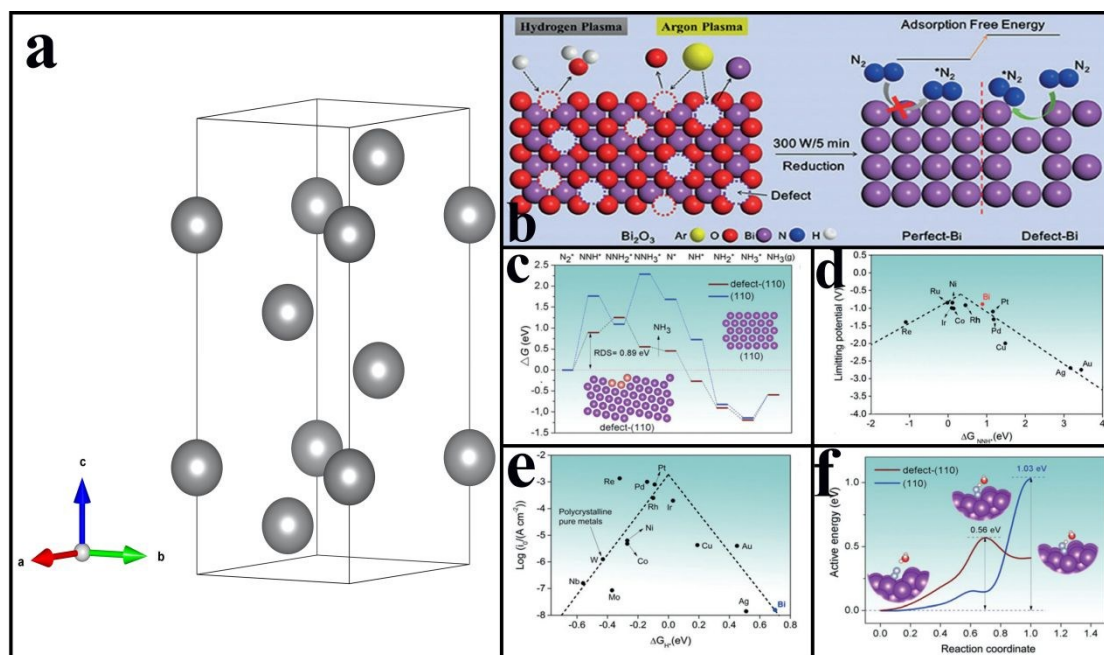
Fig. 4 (a) The crystal structure of metal Bi from standard orientation, (b) Illustration of the synthesis of defect-rich Bi nanoplates and their application for the N_2 reduction reaction, (c) The free-energy diagrams for the N_2 reduction reaction on Bi(110) and defective Bi(110) facets via a reaction pathway, and (d) Limiting potentials for N_2 electroreduction on each metal vs. the binding energy of N₂H*; (e) Volcano plot for the HER on representative transition metals; (f) activation energy of the rate-determining step. (b-f) Reproduced with permission.[44] Copyright 2019, Wiley-VCH.

3.2 Bismuth Oxide

Previously, δ-Bi_2O_3 and BiO have been reported to be active for N_2 fixation under ambient condition.[12, 45, 46] **Fig. 5a** shows the defective fluorite-prototype of δ-Bi_2O_3, which belongs to the cubic crystal system (a = b = c = 5.53 Å) and Pn3m (224) space group. Different from CaF_2, here are only 6 oxygen ions present in the stoichiometric compound to occupy the 8 equivalent anion sites, leaving 25% of the oxygen lattice sites intrinsically vacant.[47] Such natural oxygen-vacancy structure may lead to superior catalytic performance (**Fig. 5b**). The valence band of δ-Bi_2O_3 is about 2.60 eV (vs. NHE) and its conduction band is about -0.25 eV (vs. NHE), which is not energetically accessible to N_2 reduction. Due to the oxygen vacancies in δ-Bi_2O_3, N_2 can be chemically adsorbed in the vacancies and then activated by the photogenerated electrons, which makes the δ-Bi_2O_3 based photocatalysts have excellent performance in photocatalytic N_2 reduction.[45, 46]

BiO is another bismuth oxide with superior performance in photocatalytic N_2 reduction. The crystal structure of BiO from standard orientation in **Fig. 5c** shows that it has a trigonal crystal system (a = b = 3.88 Å, c = 9.71 Å) and R3m (160) space group. BiO shows a hexagonal tunnel structure along the (010) direction, arranged by Bi and O groups. More importantly, the size of the "tunnel" in the BiO crystal structure is around 4.5 Å and it is much larger than the diameter of N_2 molecules. Consequently, N_2 can be caged in BiO and further activated. According to density functional theory (DFT) calculation, the valence bands of BiO near Fermi levels are mainly generated by

p-electrons of Bi atoms (**Fig. 5d, e**). The charge distribution on the surface of BiO (010)

can be accumulated near the Bi atoms, which means that Bi atoms can provide electrons

as active centres. This is the main reason why the BiO photocatalyst exhibits excellent

N_2 reduction performance (1226 μmol/g/h, which is one thousand times higher than

iron-doped TiO_2).[12] Due to the lone pair of electrons on the Bi atom, N≡N can be

stretched by three alternatively arranged Bi atoms via donating electrons to the empty

6d orbitals of Bi and accepting electrons from the lone pairs of Bi atoms to the

unoccupied σ^*2p_x, π^*2p_y and π^*2p_z orbitals. The obtained electrons from the three

adjacent low valence Bi ions can strongly weaken the N≡N, which leads to a one-step

three electron N_2 reduction process (**Fig. 5f**).
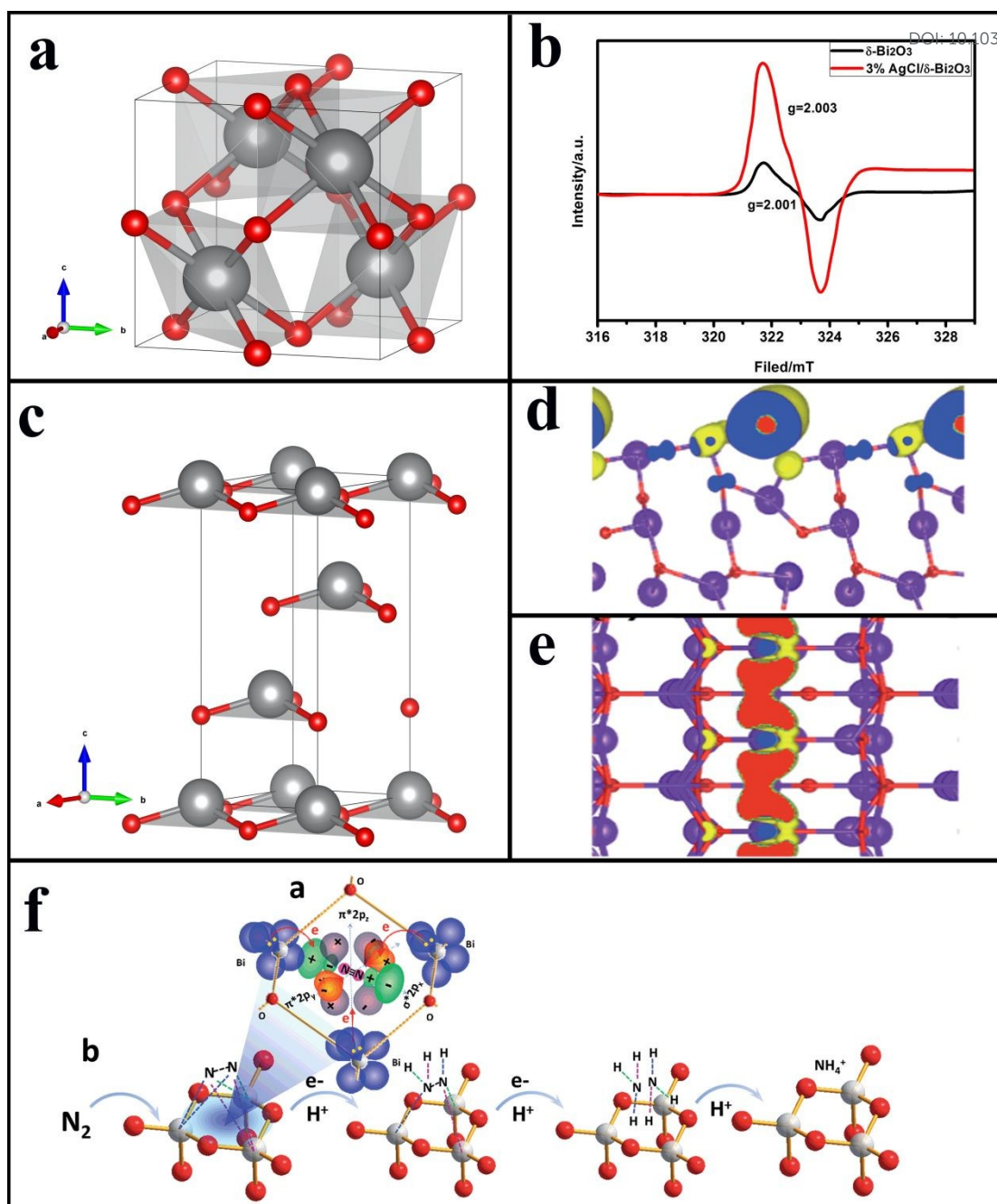
Fig. 5 (a) The crystal structure of δ-Bi$_2$O$_3$ from standard orientation. (b) EPR spectra of δ-Bi$_2$O$_3$ and 3% AgCl/δ-Bi$_2$O$_3$. (c) The crystal structure of BiO from standard orientation. The calculated charge density plot at the valence band maximum (VBM) of BiO (010) surfaces; (d) top view and (e) side view. (f) Possible pathway for N$_2$ activation and hydrogenation on the BiO catalyst. (b) Reproduced with permission.[45] Copyright 2019, Elsevier. (d-f) Reproduced with permission.[12] Copyright 2017, Royal Society of Chemistry.

3.3 Bismuth oxyhalides

Bismuth oxyhalides are typical ternary semiconductors belonging to the tetragonal

Materials Horizons Accepted Manuscript

crystal system and P4/nmm (129) space group. They generally have the formula of $[Bi_lO_mX_n]$, in which X = Cl, Br or I. The specific Bi oxyhalide structure can facilitate the formation of a layered structure comprising $[Bi_lO_m]$ and $[X_n]$ monolayers. In $[Bi_lO_m]$ layers, Bi and O are connected by covalent bonds, and van der Waals forces exist between $[Bi_lO_m]$ and $[X_n]$ (**Fig. 6a**).[48] In general, it is very difficult for N_2 molecules to be chemically adsorbed on the surface of bismuth oxyhalides because of their poor interaction between their surface and N_2 molecules.[49] Recently, it has been confirmed that creating oxygen vacancies on the surface of bismuth oxyhalides is a highly efficient approach to improve the photocatalytic N_2 reduction performance (**Fig. 6b**).[13, 50-52] For instance, BiOBr without oxygen vacancies nearly has no N_2 reduction performance, while 1 g of BiOBr with oxygen vacancies can generate 104.2 μmol ammonia in an hour under visible light (λ **>** 420 nm) irradiation.[22] It is attributed to the fact that oxygen vacancies can feed local electrons back to the π antibonding orbital of N_2 molecules and adsorb them tightly.[22, 49] Meanwhile, the strong interaction between the Bi $6p$ band the N $2p$ orbitals can further enhance the adsorption, which is crucial for the cleavage of N≡N and the activation of N_2.[27]
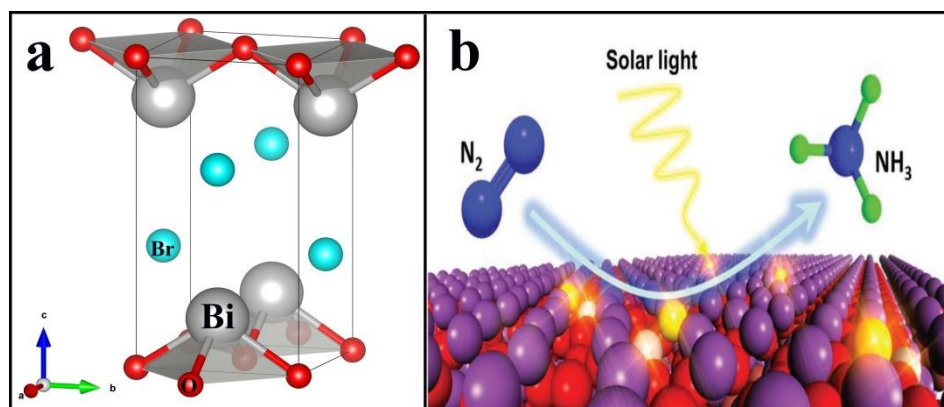

Fig. 6 (a) The crystal structure of BiOBr from standard orientation; (b) schematic illustration of the photocatalytic N_2 fixation over defect-rich Bi_3O_4Br. (b) Reproduced with permission.[52] Copyright 2019, Wiley-VCH.

3.4 Bi-based polyoxometalates

The polyoxometalates consist of three or more transition metal oxyanions linked together by shared oxygen atoms to form closed 3-dimensional frameworks. The metal atoms are usually Mo, W or V in their high oxidation states. Bi_2MoO_6 belongs to the monoclinic crystal system (a = 5.51 Å, b = 16.23 Å, c = 5.49 Å) and P b c a (61) space group, sandwiched by the $(Bi_2O_2)^{2+}$ between the perovskite-like MoO_6 octahedral layers (**Fig. 7a**).[53] The conduction band (CB) bottom and valence band (VB) top of Bi_2MoO_6 are at -0.19 and +2.29 eV, which is very close to E(N_2/NH_3 vs. NHE).[54] Generally, it is challenging to carry out the N_2 reduction reaction on the surface of Bi_2MoO_6 as the CB is not sufficiently negative. Hao et al. stated that the coordinating unsaturated Mo atoms exposed at the edges of the Mo-O coordination polyhedron could become the active centre of the N_2 adsorption, activation and photocatalytic reduction. There are two main reasons for the excellent catalytic performance of the Bi_2MoO_6: (i) the strong chemisorption between the N_2 and Mo active centres enables to eliminate the spatial deferral of electron transmission, and (ii) the space barriers of exciton donor centre and active centre can minimise the high overlap between the active centre and CB of Bi_2MoO_6.[21]

Besides, bismuth vanadate is another catalyst that can be used for N_2 fixation under ambient environment. $BiVO_4$ belongs to the monoclinic crystal system (a = 5.19 Å, b = 5.09 Å, c = 11.70 Å) and I112/b (15) space group, which consists of BiO_8 and VO_4

groups. $BiVO_4$ is a layered material that is vertically separated in the c direction by rickety bonded oxygen planes (**Fig. 7b**). The CB bottom and VB top of $BiVO_4$ are at +0.02 and +2.53 eV (vs. NHE), indicating that the productivity of photocatalytic generated electrons in the CB of $BiVO_4$ is too weak to reduce N_2.[55] The results show that the external electric field can reduce the energy barriers and make N_2 fixation reaction on the surface of bismuth vanadate catalysts possible.[26, 56] DFT simulation indicates that the CB of $BiVO_4$ is mainly composed of V $3d$ states, and the Bi $6p$ states contribute to the top.[57] Like bismuth oxyhalides and Bi_2MoO_6, N_2 molecules are challenging to be adsorbed on the prefect crystal surface of $BiVO_4$. With oxygen vacancies induced to the structure of $BiVO_4$, the V atoms with low coordination undergo spin-polarisation, which contributes to the activation and cleavage of N_2 molecules. Compared with clean $BiVO_4$, the N_2 adsorption energy on $BiVO_4$ with oxygen-vacancy reduced by 0.2 eV, indicating much stronger chemical adsorption. More importantly, the high spin-polarisation can stretch the N≡N from 1.117 to 1.143 Å, resulting in a facile split of N_2 molecules.[56]
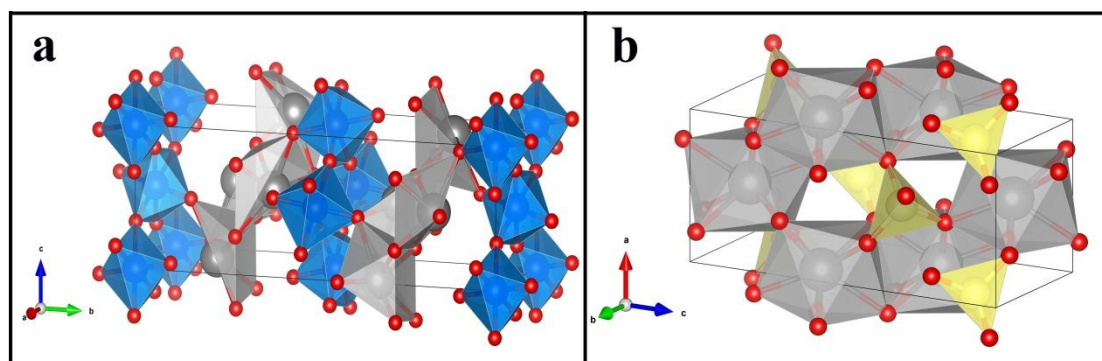
**Fig. 7** The crystal structure of (a) Bi_2MoO_6 and (b) $BiVO_4$.

4. Modification strategies

4.1 Surface oxygen-vacancy engineering

Oxygen vacancy is a kind of common defect in materials which can significantly influence the properties of the materials by causing lattice distortions and excess-electron distribution[58], which is recognized as the fingerprint of the electronic structure of materials. The aims of surface oxygen-vacancy engineering are to control the concentration of vacancies and the nature of materials, with the hope of improving the properties of materials in the desired manner, even introducing some unexpected properties.[59] In the catalytic field, oxygen vacancies are usually the most reactive sites on the catalyst surface, as it binds the adsorbate more strongly than normal oxide sites and aid their cleavage. More importantly, the induced oxygen vacancies can change the charged nature and the band-bending of electron-hole pairs.[60] So far, the generation of oxygen vacancies on the surface of Bi-based materials is the most widely used approach to satisfy the N_2 fixation reaction. For example, oxygen vacancies on BiOBr can directly trap photoexcited electrons and reduce the recombination of electron-hole pairs. Meanwhile, the N_2 molecules are strongly chemisorbed, after which the electrons will be fed back to the antibonding π^* orbitals of N_2, and the $N\equiv N$ will be activated (**Fig. 8a**).[22] Wang et al. reported ultrafine Bi_5O_7Br nanotubes with excellent photocatalytic N_2 fixation performance. They found that some O atoms could escape from the surface of Bi_5O_7Br, leaving some oxygen vacancies that could adsorb and immobilise the N_2 molecules. Interestingly, the photoinduced oxygen vacancies can be refilled with water,

which returns well to the original stable state (**Fig. 8b**).[50] The function of oxygen vacancies of Bi-based materials is summarised as follows: (i) oxygen vacancies can bind N_2 molecules, provide localised electrons in the reverse direction, reduce the adsorption energy and strongly chemisorb the N_2 on the surface of catalysts; (ii) the strong interaction between the Bi $6p$ band the N $2p$ orbitals can ulteriorly strengthen the adsorption of N_2 molecules; (iii) the accumulated electrons can take part in the activation and cleavage reaction of N_2, which is the rete-determining step for N_2 fixation; (iv) the introduction of oxygen vacancies can broaden the light absorption and narrow the bandgap of the catalysts.

Nevertheless, too many defects may cause opposite effects. For instance, Chen et al. employed ball milling method to create some defects on the surface of ZnO and the photocatalytic performance of ZnO significantly decreased.[61] This kind of circumstance can also occur in Bi-based materials. Zhu et al. found that ball milling can reduce the photocatalytic activity of $BiPO_4$ and they realised that reflux in water can repair the defects.[62] All in all, a suitable amount of defects can enhance the catalytic performance of materials. Unfortunately, accurate amounts of defects cannot be obtained through currently available technologies. For different materials, they may acquire different amounts of defects to achieve optimum catalytic activity and this issue should be explored via a large number of tedious experiments.
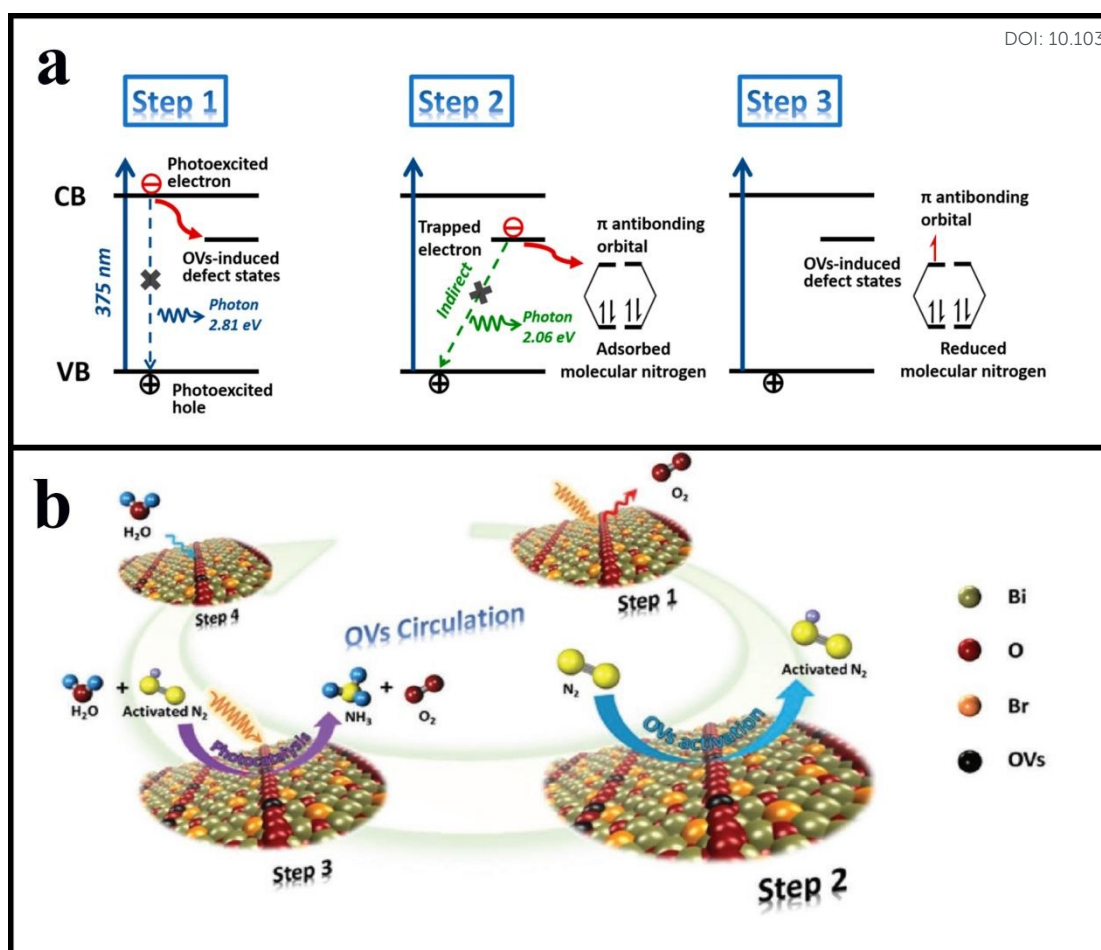
Fig. 8 (a) Schematic illustration for enhanced interfacial electron transfer processes induced by oxygen vacancies of BiOBr, (b) Schematic illustration of the photocatalytic N_2 fixation model in which water serves as both the solvent and proton source, as well as the reversible creation of light-induced oxygen vacancies. (a) Reproduced with permission.[22] Copyright 2015, American Chemical Society. (b) Reproduced with permission.[50] Copyright 2017, Wiley-VCH.

4.2 Surface molecules grafting

Surface molecules grafting is a highly efficient strategy to trim the surface charge distribution of catalysts and enhance their catalytic performance.[28, 63, 64] For example, Min et al. modified the porous g-C_3N_4 by adsorbing Eosin Y on its surface and the light absorption edge was expanded to 600 nm. Besides, the photocatalytic activity for hydrogen generation of modified g-C_3N_4 is much higher than that of pure g-C_3N_4, and

the apparent quantum efficiency under 550-nm light irradiation is 19.4%.[65] In the same

way, the surface molecules grafting is also effective for the N_2-fixation catalysts.

Bi_2WO_6 has no significant photocatalytic N_2 fixation performance, while the N_2-

fixation rate can be 140 μmol/g/h after grafting cyclized polyacrylonitrile heterocycles

to its surface.[66] The pyridinic N in cyclized polyacrylonitrile can turn into the

unsaturated state, which can bind with N_2 molecules and donate electrons (**Fig. 9**). As

a result, the adsorption capacity and activation rate of N_2 are both greatly enhanced.

Surface molecules grafting is certainly an effective approach to achieve higher N_2

reduction performance. However, the design of such catalysts still has a lot of

challenges. Firstly, it is difficult to select a proper kind of molecule which can benefit

the catalysts and this step requires a high amount of theoretical calculation. Secondly,

it is challenging to graft the selected molecules to the surface of catalysts. Besides,

extensive experiments should be carried on to make sure the optimum grafting amount.

The stability of catalysts is also crucial for their application, and thus the stability of

grafted molecules should also be considered.
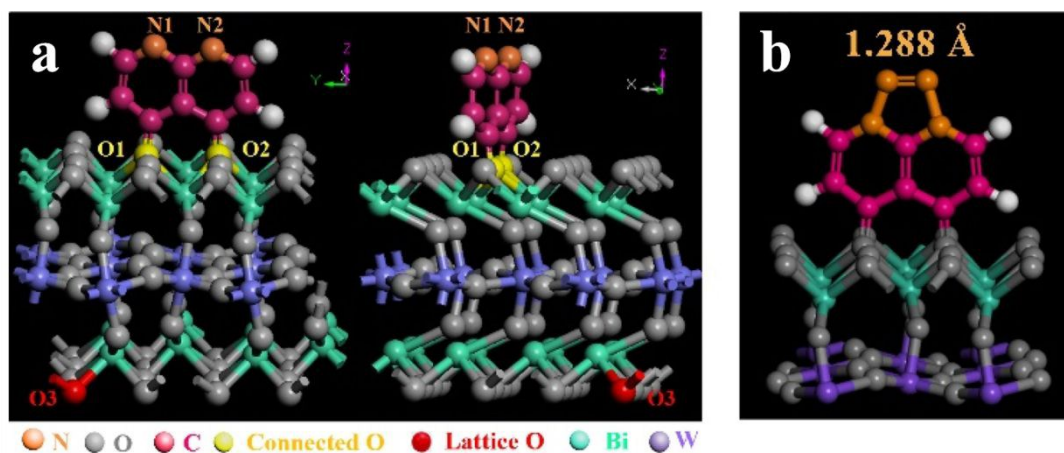
Fig. 9. Characterisation and calculation of surface bonding state of (a) Bi_2WO_6 and (b) adsorbed N_2 molecule bond length of Bi_2WO_6/cyclized polyacrylonitrile hybrid photocatalysts. (a, b) Reproduced with permission.[66] Copyright 2018, American Chemical Society.

4.3 Regulation of internal electric field

The internal electric field is usually generated by the polarisation of the nonuniform charge distribution between various constituent layers, and its generation and regulation is another essential approach to enhance the activity of catalysts.[48] It can be formed via ferroelectric effect, heterojunctions, or polar surface terminations.[67] For the distinctive layer structure, strategies can be applied to regulate the internal electric field of bismuth oxyhalides and Bi_2MoO_6. For instance, Li et al. prepared single-crystalline Bi_3O_4Cl nanosheets with a high percentage (001) facet exposure and found that a large amount of (001) facet exposures can generate a stronger internal electric field, which can accelerate the transfer and separation of photogenerated charge carriers.[68] In addition to regulating the structure of single-component nanomaterials, the generation of internal electric fields between two heterostructure interfaces is also an effective strategy to improve catalytic performance.[69] Lv et al. found that the introduction of amorphous CeO_2 to $Bi_4V_2O_{11}$ can lead to band bending and an active internal electric field can be formed, which is conducive to the electrocatalytic N_2 reduction (**Fig. 10a**). The catalytic activity of $CeO_2/Bi_4V_2O_{11}$ is much higher than the other catalysts (**Fig. 10b**). The NH_3 yield rate reached 23.21 ug/mg/h, and the Faradaic efficiency was 10.16%. Besides, the high-valence Bi defects can take oxygen away from $[VO_{3.5}]^{2-}$ layers, resulting in the enrichment of oxygen vacancies. As a result, the cleavage of N_2 molecules is significantly enhanced by the π electron back donation.[26]

The current technology is though not enough for quantitative analysis the amount

of internal electric field. If the dynamic relation between the amount of internal electric field and the catalytic activity can be clearly clarified, it will be a significant progress in designing high-performance catalysts. At the same time, it is still difficult to identify two kinds of semiconductors with well-match band structures and surfaces.
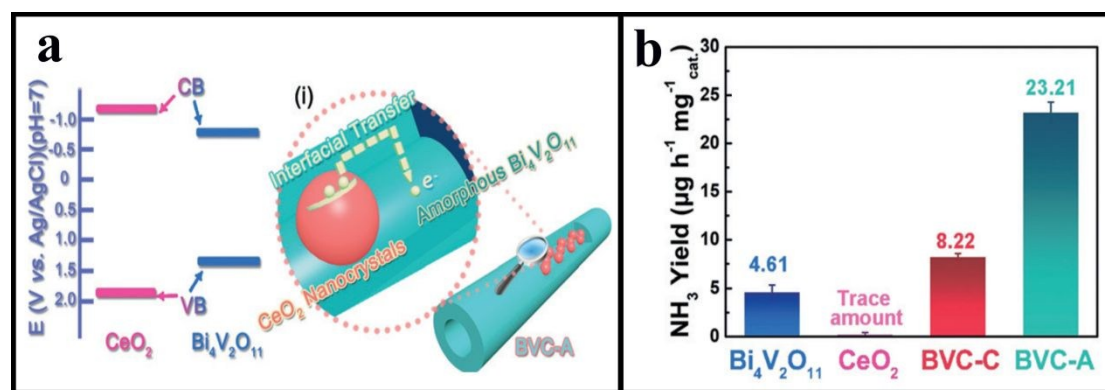
Fig. 10 (a) Illustration of interfacial charge transfer in $CeO_2/Bi_4V_2O_{11}$. (b) Yield of NH_3 with various catalysts. (a, b) Reproduced with permission.[26] Copyright 2018, Wiley-VCH.

4.4 Developing Air-Liquid-Solid triphase Interfaces

Very recently, developing air-liquid-solid triphase interface to increase catalytic performance has attracted significant interests.[70-72] Sheng et al. reported a novel triphase photocatalytic system where TiO_2 was immobilised on the surface of a superhydrophobic porous polytetrafluoroethylene substrate (**Fig. 11a**). The unique triphase photocatalytic system shows 10-fold enhancement on the degradation of organic pollutant than traditional liquid/solid diphase system. This is due to the fact that a distinctive airbag structure can be formed on the surface of the superhydrophobic substrate in wastewater, which can rapidly deliver oxygen to the reaction system as a natural electron scavenger. Different from the traditional liquid/solid diphase system,

oxygen can be rapidly obtained from air and delivered to the reaction system rather than

dissolved in liquid. Therefore, both the photocatalytic kinetics and pollutant

degradation rate are significantly enhanced. Similarly, such a triphase system can also

be effective in CO_2 reduction or N_2 fixation reaction as it can greatly improve the

contact area between the catalysts and gases. Liu et al. prepared $Bi_4O_5Br_2$/ZIF-8

composite, and its photocatalytic N_2 reduction efficiency was 3.6 times higher than that

of $Bi_4O_5Br_2$.[73] The CB and VB of $Bi_4O_5Br_2$ are at 0.21 and 2.51 eV, while those of ZIF-

8 are at -0.81 and 4.4 eV, thus it is impossible for these two materials to form a

heterojunction to accelerate the separation of electron-hole pairs. The triphase interface

created by the hydrophilic-hydrophobic structure of $Bi_4O_5Br_2$/ZIF-8 can directly

deliver N_2 from air to the photocatalytic reaction system, thereby significantly

improving the contact between the catalyst and N_2 molecules, and the photocatalytic

nitrogen fixation performance (**Fig. 11b**).

Currently, only a few air-liquid-solid triphase interface systems have been

reported. There are actually still a lot of barriers in the design of these unique systems.

On the one hand, the base is always consisted with superhydrophobic materials and it

is difficult to make semiconductors stably grown on their surface, thus the triphase

interface systems usually do not have very good stability. On the other hand, the proper

loading amount, the cost and the synthetic simplicity should be carefully considered in

combination.
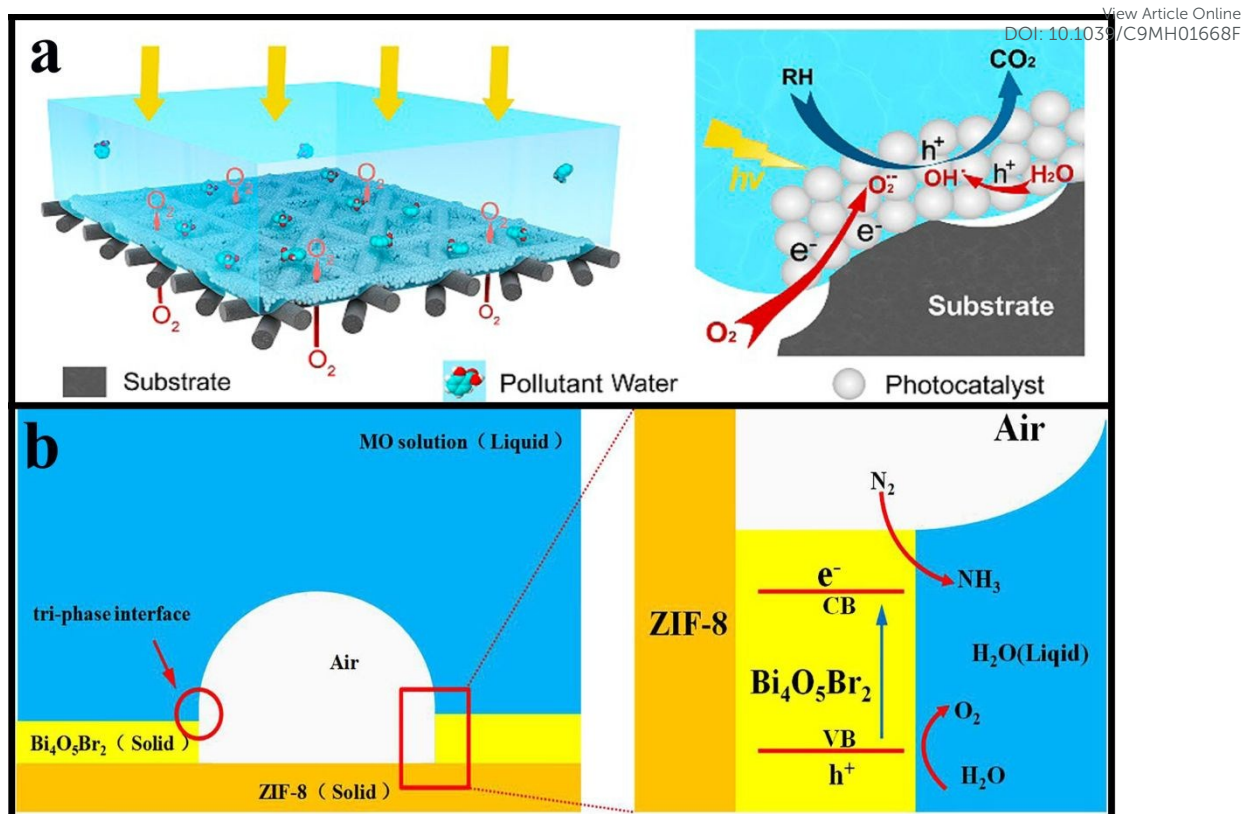
Fig. 11 (a) Schematic illustration of the triphase photocatalytic system. (b) Photocatalytic mechanism of $Bi_4O_5Br_2$/ZIF-8. (a) Reproduced with permission.[71] Copyright 2017, American Chemical Society. (b) Reproduced with permission.[73] Copyright 2019, Elsevier.

5. Principles of constructing high-performance bismuth-based catalysts for N_2 fixation

Whatever electrocatalysis or photocatalysis, the transfer speed of electrons is crucial for the reaction. If the conductivity of the electrode material of the electrocatalyst is not good, the external circuit needs to load additional voltage to drive the effective transmission of electrons in the whole reaction system, thus greatly reducing the activity of the materials. The reason is that the completion of N_2-fixation reaction requires the continuous adsorption, reaction and desorption process on the active sites, for which the charge transfer is the key factor. The key barriers on the way

of the application of photocatalysis are the rapid recombination of photogenerated electron-hole pairs and the low utilization ratio of solar energy. Approaches should be employed to control the bandgap and band structure to achieve excellent N_2 fixation performance. Elements doping and creating heterojunctions are probably to provide significant effects in this aspect. In comparison, for electrocatalysis, the electric field is employed to induce the adsorption and conversion of molecules, and strategies should be taken to improve the conductivity of materials, the adsorption and activation of molecules. Currently, the modification with carbon-based materials, the regulation of nanostructure, and the surface modification may be more helpful.[22, 37, 74, 75]

Overall, Bi-based catalysts have the shortages of low transfer speed of electrons and poor stability. Besides, the CB position of some Bi-based photocatalysts is not negative enough to achieve a high reduction performance. Therefore, effective strategies should be selectively employed to overcome these key issues when designing Bi-based materials for N_2 fixation. Based on the crystal structure and natural properties of the Bi-based materials, several key principles can be employed to reduce the influence of the affecting issues, in order to construct high-performance catalysts for N_2 fixation.

Metallic Bi belongs to metal crystal, in which the arrangement of atoms is not regular and complete, and there are often areas that deviate from the ideal structure. Therefore, there are always some defects in the crystal structure of metallic Bi, which may lead to the change of surface charge distribution and stronger adsorption of N_2 molecules. However, it is changeling to accurately evaluate and control the amounts of

defects. Besides, the surface of metallic Bi can be easily oxidised and form a thin layer of bismuth oxide, which probably impede the adsorption and activation of N_2 molecules.[76] With different raw materials and different reductants, metallic Bi with various structures and different amounts of defects can be obtained. At this time, electron paramagnetic resonance technology can be employed to compare the relative defect concentration. As for the unavoidable surface oxidation, core-shell structures can be synthesised by surface coating of metal oxides or metal-free materials, which can significantly reduce the oxidation of metallic Bi.

Bismuth oxides have several phases, among them, only δ-Bi_2O_3 and BiO have been confirmed to be used as N_2-fixation catalysts.[12, 37, 45] The typical oxygen defects of δ-Bi_2O_3 and the natural tunnels of BiO can make N_2 molecules strongly adsorbed on the surface of catalysts, which is beneficial for the catalytic reaction. However, the poor stability of bismuth oxides significantly limits their application.[77] The stability is related to the spatial arrangement diversity of (BiO_5) structural units, which can be improved by elements doping.[78] Therefore, strategies focusing on the kinds of elements, doping methods and doping amounting should be carried on to improve the stability of bismuth oxides.
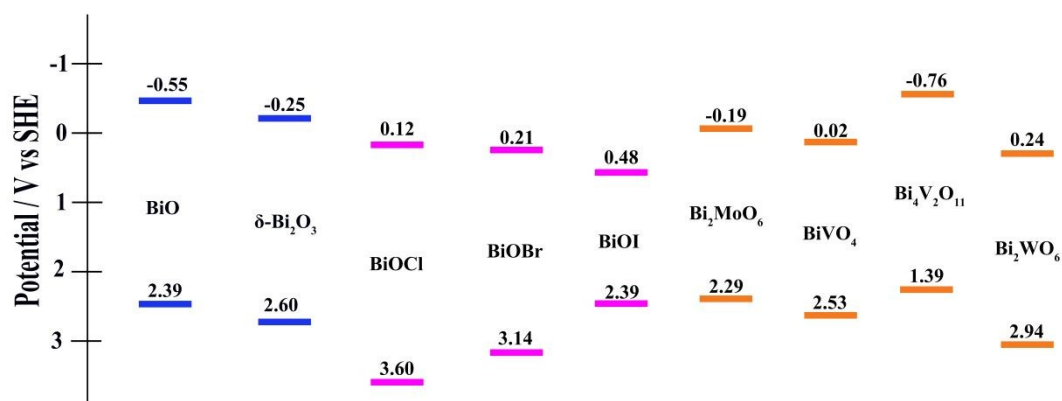
Fig. 12 The band structure of Bi-based semiconductors including bismuth oxides, bismuth oxyhalides and Bi-based polyoxometalates.

Bismuth oxyhalides and Bi_2MoO_6 are all compounds with a layered structure. It is relatively easy to control the nanostructure, change the exposed crystal planes and regulate their internal electric fields to reach higher photocatalytic performance.[22] Nevertheless, the conduction bands of these materials, especially bismuth oxyhalides and $BiVO_4$, are not negative enough to achieve ideal reduction reaction (**Fig. 12**). It must be noted that the van der Waals forces between the layers are not strong, and the diversity of spatial arrangement of (BiO_5) structural units of the materials can lead to the instability of bismuth oxyhalides and Bi_2MoO_6.[48, 78] Such circumstances may be improved by proper element doping. In the N_2 reduction process, the electrons may react with Bi^{3+} and generating Bi^0, changing the component and performance of catalysts. The mentioned approaches which can accelerate the transfer of electrons may also help avoid the reduction of Bi^{3+}. The position of CB of materials determines their reduction ability. To improve the reduction ability of Bi-based photocatalysts, elements doping, creating heterojunction and surface oxygen vacancy engineering may be helpful.[79-83]

Both the diversity of spatial arrangement of (BiO_5) structural units and the reduction of Bi^{3+} can cause the instability of Bi-based catalysts. Elements doping can not only change the surface charge distribution and improve the catalytic performance, but also stabilize the (BiO_5) structural units.[78] Thus it is an efficient way to modify Bi-based catalysts to be more stable and more effective.[84, 85] The reduction of Bi^{3+} can be

avoided by accelerating the transfer of electrons in the reaction system. For instance,

Guan et. al prepared a z-scheme $BiVO_4$-AgI photocatalysts, which exhibited higher

photocatalytic activity and enhanced stability. The enhanced stability is attributed to

the significantly accelerated transfer of electrons in the heterojunction.[86]

Ag_3PO_4/BiOBr heterojunction with similar function has also been reported.[87] Besides,

surface modification may also be helpful. Hao et. al found that surface halogenation

can greatly enhance the photocatalytic CO_2 reduction of bismuth oxyhalides. More

importantly, this facile surface halogenation can significantly improve the transfer and

delivery of electrons, avoiding the reduction of Bi^{3+}.[88] Therefore, the surface

halogenation improved the stability of bismuth oxyhalides. In addition to creating

heterojunctions and surface halogenation, similar approaches to achieve rapid transfer

of electrons, such as surface modification with carbon-based materials and dye-

sensitization may also be effective to improve the stability of Bi-based catalysts for

ammonia synthesis.
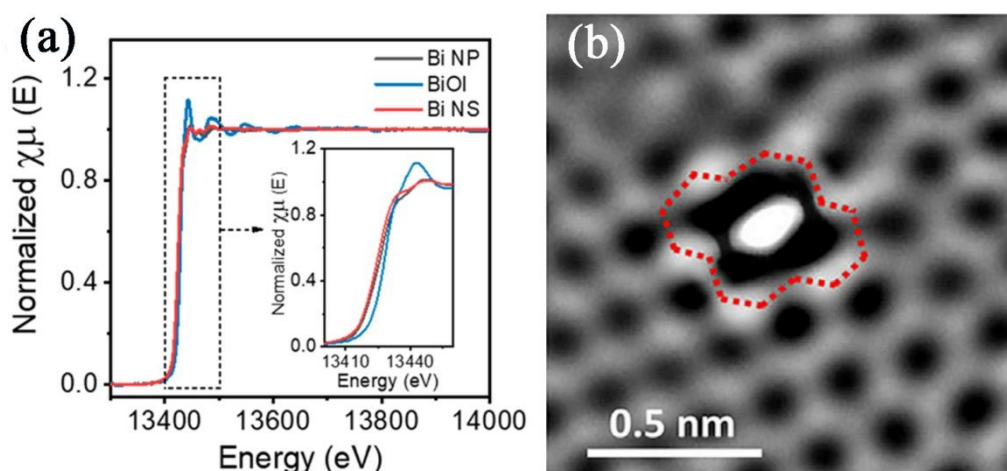
Fig. 13 (a) Bi L_{III}-edge XAFS of BiOI precursor, Bi nanosheets, and Bi nanoparticles. Reproduced with permission.[11] Copyright 2019, American Chemical Society. (b) HADDF-STEM image of atomic Ni

The development of advanced characterization technologies can help researchers better understand the fine nanostructure of materials, and may deepen the understanding of the reaction mechanisms. In the catalytic area, X-ray absorption fine spectroscopy (XAFS) is usually used to characterize the geometry and electronic structure of the catalysts. With XAFS, we can get a lot of essential structural information of materials, including the valence states of elements, coordination charges, orbital hybridization, coordination number, symmetry, bond length, disorder factor, etc.[90-92] It has been widely applied in the studies of Bi-based materials for ammonia synthesis. For example, Li et. al prepared metallic Bi nanosheets by the reduction of BiOI. In the XAFS of the samples, BiOI is in higher oxidation state and it has an obvious higher energy of the Bi L_{III} edge. While for the reduced metallic Bi nanosheet, it has a lower absorption energy and it matches the edge of metallic Bi particles, indicating that the BiOI has been completely converted to metallic Bi.[11] Hao et. al also studied the metallic Bi for the electrocatalytic synthesis of ammonia, and they used in situ X-ray absorption near-edge spectroscopy to study the change of the catalysts during the electrochemical reaction process.[27] They found that the active species during the electrocatalytic reactions is Bi^0 and it can keep thermodynamically stable phase during the reaction.

Compared with traditional transmission electron microscopy (TEM), aberration-corrected high-angle annular dark-field scanning transmission electron microscopy (HAADF-STEM) has much better resolution, which significantly enhanced atomic-level observation and atomic-level analysis capabilities.[93, 94] With HAADF-STEM, we

can learn more about the atomic level of materials. If we can accurately control the

atomic-level structure of materials, the performance of nanomaterials will reach a new

platform. For example, Zhang et. al reported a kind of atomic Ni trapped with graphene

defects catalyst, which showed excellent performance of electrochemical water

splitting. The size of atomic Ni is only about 0.25 nm, which cannot be observed by

traditional TEM. It also has good application in Bi-based materials.[89] Zhang et. al

prepared bismuth single atoms with the transformation of metal-organic frameworks,

and the single-atom electrocatalyst exhibited high Faradaic efficiency (97%) for the

reduction of CO_2.[95] According to the results of HAADF-STEM and DFT calculation,

the authors found that the single-atom $Bi-N_4$ site are active centre for CO_2 activation.

In the future, advanced technologies such as XAFS and HAADF-STEM will provide

more solid evidence for the study of Bi-based materials for ammonia synthesis.

6. Summary and outlook

The main obstacles to the development of artificial N_2 reduction include the

solubility of N_2 in aqueous, the stable chemical nature of N_2, and the competitive

reaction of HER. Bi-based catalysts with controllable structure and surfacing

engineering have great potential for solving these problems.

Increasing the solubility of N_2 is an effective method for the improvement of N_2

reduction since the electrocatalytic ammonia yield rate, and Faradaic efficiency can be

enhanced. Ionic liquids like $[C_4mpyr][eFAP]$ and $[P_{6,6,6,14}][eFAP]$ have been used as

electrolytes to increase N_2 solubility. However, these two ionic liquids are costly and therefore not suitable for mass application.[96] The development of air-liquid-solid triphase interface can be used as a facile and effective way to significantly increase the rate of the N_2 reduction reaction. In this unique system, an airbag structure can be formed on the surface of the superhydrophobic substrate. Thus N_2 from the air can be rapidly and continuously delivered to the reaction system. Meanwhile, the contact area and time between the catalysts and N_2 are greatly increased, leading to high N_2 reduction reaction rate. Also, the triphase system is much less expensive than ionic-liquid electrolytes. Due to the strong interaction between the Bi $6p$ band the N $2p$ orbitals, N_2 molecules can be adsorbed on the surface of Bi-based catalysts, especially the one with oxygen vacancies. δ-Bi_2O_3 is a defective fluorite-prototype structure and its natural oxygen vacancies can facilitate the adsorption and activation of N_2. More importantly, the oxygen vacancies can lead to the accumulation of electrons on the surface of catalysts, which can feedback to N_2 and weaken the N≡N. The natural tunnel of BiO can also enhance the adsorption of N_2. Because HER requires a more negative potential than N_2 reduction, overcoming HER competitiveness is a big challenge. Notably, Bi is a less reactive metal that promotes the selectivity of N_2 activation without changing the binding energy of further intermediates. At the same time, the surface electron accessibility of HER can be prevented as it has poor hydrogen adsorption energy.[11, 97] Based on the mentioned characteristics, Bi-based materials exhibit great potential in artificial ammonia synthesis under ambient condition. However, the shortages of low transfer speed of electrons, poor stability and positive CB position are

the barriers for a new platform. Thus, effective strategies should be employed to minimise the influence of these weaknesses.

Developing environmentally friendly and highly efficient artificial ammonia synthesis is crucial to reducing CO_2 emission and releasing global warming. Surface oxygen-vacancy engineering of Bi-based catalysts has proven to be an effective method to achieve unique N_2 reduction performance as it enhances the adsorption and activation of N_2. Surface oxygen vacancies and grafted molecules can regulate the surface charge distribution, adsorb N_2 molecules and act as active sites. However, if there are too many oxygen vacancies, the transfer of electrons may be hindered. An appropriate amount of oxygen vacancies can maximise the catalytic performance, but current techniques are unable to obtain the accurate concentration of vacancies in materials. It is urgent to understand the mechanism of defect formation, accurately control the number of defects, and study its effect on nitrogen fixation activity. As for surface molecules grafting, it may refer to some toxic chemicals and complex operations. Regulation of the internal electric field of Bi-based materials can accelerate the transfer and separation of electron-hole pairs, adjust the charge distribution, and improve the N_2 fixation performance. However, there is still a lack of methods for accurately measuring and controlling the amount of internal electric field. Developing air-liquid-solid triphase interface is an inexpensive and effective approach to increase the concentration of N_2 in the reaction system and thereby improve the catalytic performance. However, designing a more concise, stable and low-cost system remains a challenge.

As global warming becomes more serious, it is imperative to use Bi-based

35

catalysts for artificial ammonia synthesis to reduce CO_2 emission under ambient condition. Metallic Bi, bismuth oxide, bismuth oxyhalides and Bi-based polyoxometalates all performed excellent artificial N_2-fixation activity. However, the ammonia yield is too low to meet the mass production needs. Some modification approaches such as surface oxygen-vacancy engineering, surface molecules grafting, regulation of internal electric field and developing air-liquid-solid triphase have great potential in solving the problems. Advanced technologies such as XAFS and HAADF-STEM will help us get more detailed structure of Bi-based materials and better reveal the reaction mechanism. Bi-based materials may make the nitrogen fixation dream alive, but here is still a long way to go.

Conflicts of Interest

The authors declare no conflicts of interest.

Acknowledgement

Reference

1.   L. Lassaletta, G. Billen, B. Grizzetti, J. Anglade and J. Garnier, *Environ. Res.*

Lett., 2014, **9**, 105011.

2. N. G. Polikhronidi, I. M. Abdulagatov, R. G. Batyroua and G. V. Stepanov, *Int. J. Refrig.-Rev. Int. Froid*, 2009, **32**, 1897-1913.

3. S. Giddey, S. P. S. Badwal and A. Kulkarni, *Int. J. Hydrog. Energy*, 2013, **38**, 14576-14594.

4. J. P. Guo and P. Chen, *Chem*, 2017, **3**, 709-712.

5. T. Kandemir, M. E. Schuster, A. Senyshyn, M. Behrens and R. Schloegl, *Angew. Chem. Int. Ed.*, 2013, **52**, 12723-12726.

6. G. J. Leigh, *Catalysts for Nitrogen Fixation: Nitrogenases, Relevant Chemical Models and Commercial Processes*, 2004, 33-54.

7. B. E. Smith, *Science*, 2002, **297**, 1654-1655.

8. C. W. Liu, Q. Y. Li, C. Z. Wu, J. Zhang, Y. G. Jin, D. R. MacFarlane and C. H. Sun, *J. Am. Chem. Soc.*, 2019, **141**, 2884-2888.

9. C. W. Liu, Q. Y. Li, J. Zhang, Y. G. Jin, D. R. MacFarlane and C. H. Sun, *J. Mater. Chem. A*, 2019, **7**, 4771-4776.

10. C. W. Liu, Q. Y. Li, J. Zhang, Y. G. Jin, D. R. MacFarlane and C. H. Sun, *J. Phys. Chem. C*, 2018, **122**, 25268-25273.

11. L. Q. Li, C. Tang, B. Q. Xia, H. Y. Jin, Y. Zheng and S. Z. Qiao, *ACS Catal.*, 2019, **9**, 2902-2908.

12. S. M. Sun, Q. An, W. Z. Wang, L. Zhang, J. J. Liu and W. A. Goddard, *J. Mater. Chem. A*, 2017, **5**, 201-209.

13. X. L. Xue, R. P. Chen, H. W. Chen, Y. Hu, Q. Q. Ding, Z. T. Liu, L. B. Ma, G. Y. Zhu, W. J. Zhang, Q. Yu, J. Liu, J. Ma and Z. Jin, *Nano Lett.*, 2018, **18**, 7372-7377.

14. S. Y. Wang, F. Ichihara, H. Pang, H. Chen and J. H. Ye, *Adv. Funct. Mater.*, 2018, **28**, 1803309.

15. K. Ithisuphalap, H. G. Zhang, L. Guo, Q. G. Yang, H. P. Yang and G. Wu, *Small Methods*, 2019, **3**, 1800352.

16. X. L. Xue, R. P. Chen, C. Z. Yan, P. Y. Zhao, Y. Hu, W. J. Zhang, S. Y. Yang and Z. Jin, *Nano Res.*, 2019, **12**, 1229-1249.

17. G. N. Schrauzer and T. D. Guth, *J. Am. Chem. Soc.*, 1977, **99**, 7189-7193.

18. W. Zhao, J. Zhang, X. Zhu, M. Zhang, J. Tang, M. Tan and Y. Wang, *Appl. Cata. B-Environ.*, 2014, **144**, 468-477.

19. S. J. Li, X. Chen, S. Z. Hu, Q. Li, J. Bai and F. Wang, *RSC Adv.*, 2016, **6**, 45931-45937.

20. H. Miyama, N. Fujii and Y. Nagae, *Chem. Phys. Lett.*, 1980, **74**, 523-524.

21. Y. C. Hao, X. L. Dong, S. R. Zhai, H. C. Ma, X. Y. Wang and X. F. Zhang, *Chem.-Eur. J.*, 2016, **22**, 18722-18728.

22. H. Li, J. Shang, Z. H. Ai and L. Z. Zhang, *J. Am. Chem. Soc.*, 2015, **137**, 6393-6399.

23. K. Kugler, M. Luhn, J. A. Schramm, K. Rahimi and M. Wessling, *Phys. Chem. Chem. Phys.*, 2015, **17**, 3768-3782.

24. J. Wang, L. Yu, L. Hu, G. Chen, H. L. Xin and X. F. Feng, *Nat. Commun.*, 2018, **9**, 1795.

Materials Horizons Accepted Manuscript

25.   X. X. Yang, K. Li, D. M. Cheng, W. L. Pang, J. Q. Lv, X. Y. Chen, H. Y. Zang, X. L. Wu, H. Q. Tan, Y. H. Wang and Y. G. Li, *J. Mater. Chem. A*, 2018, **6**, 7762-7769.

26.   C. D. Lv, C. S. Yan, G. Chen, Y. Ding, J. X. Sun, Y. S. Zhou and G. H. Yu, *Angew. Chem. Inter. Ed.*, 2018, **57**, 6073-6076.

27.   Y. C. Hao, Y. Guo, L. W. Chen, M. Shu, X. Y. Wang, T. A. Bu, W. Y. Gao, N. Zhang, X. Su, X. Feng, J. W. Zhou, B. Wang, C. W. Hu, A. X. Yin, R. Si, Y. W. Zhang and C. H. Yan, *Nat. Catal.*, 2019, **2**, 448-456.

28.   D. M. Chen, K. W. Wang, W. Z. Hong, R. L. Zong, W. Q. Yao and Y. F. Zhu, *Appl. Cata. B-Environ.*, 2015, **166**, 366-373.

29.   X.-L. Ma, J.-C. Liu, H. Xiao and J. Li, *J. Am. Chem. Soc.*, 2018, **140**, 46-49.

30.   M. A. Shipman and M. D. Symes, *Cata. Today*, 2017, **286**, 57-68.

31.   J. X. Zhao and Z. F. Chen, *J. Am. Chem. Soc.*, 2017, **139**, 12480-12487.

32.   C. J. M. van der Ham, M. T. M. Koper and D. G. H. Hetterscheid, *Chem. Soc. Rev.*, 2014, **43**, 5183-5191.

33.   T. Oshikiri, K. Ueno and H. Misawa, *Angew. Chem. Inter. Ed.*, 2014, **53**, 9802-9805.

34.   J. Meija, T. B. Coplen, M. Berglund, W. A. Brand, P. De Bievre, M. Groning, N. E. Holden, J. Irrgeher, R. D. Loss, T. Walczyk and T. Prohaska, *Pure Appl. Chem.*, 2016, **88**, 265-291.

35.   P. Cucka and C. Barrett, *Acta Crystallographica*, 1962, **15**, 865-872.

36.   F. Dong, T. Xiong, Y. J. Sun, Z. W. Zhao, Y. Zhou, X. Feng and Z. B. Wu, *Chem. Commun.*, 2014, **50**, 10386-10389.

37.   Q. Hao, R. Wang, H. Lu, C. a. Xie, W. Ao, D. Chen, C. Ma, W. Yao and Y. Zhu, *Appl. Cata. B-Environ.*, 2017, **219**, 63-72.

38.   F. Dong, Z. Zhao, Y. Sun, Y. Zhang, S. Yan and Z. Wu, *Environ. Sci. Tech.*, 2015, **49**, 12432-12440.

39.   Q. Hao, Y. Liu, T. Chen, Q. Guo, W. Wei and B.-J. Ni, *ACS Appl. Nano Mater.*, 2019, **2**, 2308-2316.

40.   N. Han, Y. Wang, H. Yang, J. Deng, J. H. Wu, Y. F. Li and Y. G. Li, *Nat. Commun.*, 2018, **9**, 1320.

41.   C. A. Hoffman, J. R. Meyer, F. J. Bartoli, A. Divenere, X. J. Yi, C. L. Hou, H. C. Wang, J. B. Ketterson and G. K. Wong, *Phys. Rev. B*, 1993, **48**, 11431-11434.

42.   F. Y. Yang, K. Liu, C. L. Chien and P. C. Searson, *Phys. Rev. Lett.*, 1999, **82**, 3328-3331.

43.   J. Greeley, T. F. Jaramillo, J. Bonde, I. B. Chorkendorff and J. K. Norskov, *Nat. Mater.*, 2006, **5**, 909-913.

44.   Y. Wang, M.-M. Shi, D. Bao, F.-L. Meng, Q. Zhang, Y.-T. Zhou, K.-H. Liu, Y. Zhang, J.-Z. Wang, Z.-W. Chen, D.-P. Liu, Z. Jiang, M. Luo, L. Gu, Q.-H. Zhang, X.-Z. Cao, Y. Yao, M.-H. Shao, Y. Zhang, X.-B. Zhang, J. G. Chen, J.-M. Yan and Q. Jiang, *Angew. Chem. Intern. Ed.*, 2019, **58**,1-6.

45.   X. M. Gao, Y. Y. Shang, L. B. Liu and F. Fu, *J. Cata.*, 2019, **371**, 71-80.

46.   X. M. Gao, Y. Y. Shang, L. B. Liu and F. Fu, *J. Colloid Interface Sci.*, 2019, **533**, 649-657.

47. D. Music, S. Konstantinidis and J. Schneider, *J. Phys.-Condes. Matter*, 2009, **21**, 175403.

48. J. Li, H. Li, G. M. Zhan and L. Z. Zhang, *Accounts Chem. Res.*, 2017, **50**, 112-121.

49. H. Li, J. Shang, J. G. Shi, K. Zhao and L. Z. Zhang, *Nanoscale*, 2016, **8**, 1986-1993.

50. S. Y. Wang, X. Hai, X. Ding, K. Chang, Y. G. Xiang, X. G. Meng, Z. X. Yang, H. Chen and J. H. Ye, *Adv. Mater.*, 2017, **29**, 1701774.

51. Y. Bai, L. Q. Ye, T. Chen, L. Wang, X. Shi, X. Zhang and D. Chen, *ACS Appl. Mater. Inter.*, 2016, **8**, 27661-27668.

52. J. Di, J. Xia, M. F. Chisholm, J. Zhong, C. Chen, X. Cao, F. Dong, Z. Chi, H. Chen, Y.-X. Weng, J. Xiong, S.-Z. Yang, H. Li, Z. Liu and S. Dai, *Adv. Mater.*, 2019, **31,** 1807576.

53. Z. Dai, F. Qin, H. P. Zhao, J. Ding, Y. L. Liu and R. Chen, *ACS Catal.*, 2016, **6**, 3180-3192.

54. H. P. Li, J. Y. Liu, W. G. Hou, N. Du, R. J. Zhang and X. T. Tao, *Appl. Cata. B-Environ.*, 2014, **160**, 89-97.

55. S. J. Hong, S. Lee, J. S. Jang and J. S. Lee, *Energy Environ. Sci.*, 2011, **4**, 1781-1787.

56. J. X. Yao, D. Bao, Q. Zhang, M. M. Shi, Y. Wang, R. Gao, J. M. Yan and Q. Jiang, *Small Methods*, 2018, **3**, 1800333.

57. J. K. Cooper, S. Gul, F. M. Toma, L. Chen, P. A. Glans, J. H. Guo, J. W. Ager, J. Yano and I. D. Sharp, *Chem. Mat.*, 2014, **26**, 5365-5373.

58. M. V. Ganduglia-Pirovano, J. L. F. Da Silva and J. Sauer, *Phys. Rev. Lett.*, 2009, **102**, 4.

59. G. Pacchioni, *ChemPhysChem*, 2003, **4**, 1041-1047.

60. C. T. Campbell and C. H. F. Peden, *Science*, 2005, **309**, 713-714.

61. D. M. Chen, Z. H. Wang, T. Z. Ren, H. Ding, W. Q. Yao, R. L. Zong and Y. F. Zhu, *J. Phys. Chem. C*, 2014, **118**, 15300-15307.

62. Y. Zhu, Q. Ling, Y. Liu, H. Wang and Y. Zhu, *Appl. Cata. B-Environ.*, 2016, **187**, 204-211.

63. K. Inumaru, M. Murashima, T. Kasahara and S. Yamanaka, *Appl. Cata. B-Environ.*, 2004, **52**, 275-280.

64. B. Y. Xu, Y. An, Y. Y. Liu, B. B. Huang, X. Y. Qin, X. Y. Zhang, Y. Dai and M. H. Whangbo, *Chem. Commun.*, 2016, **52**, 13507-13510.

65. S. Min and G. Lu, *J. Phys. Chem. C*, 2012, **116**, 19644-19652.

66. C. M. Zhang, G. Chen, C. Lv, Y. Yao, Y. L. Xu, X. L. Jin and Q. Q. Meng, *ACS Sustain. Chem. Eng.*, 2018, **6**, 11190-11195.

67. L. Li, P. A. Salvador and G. S. Rohrer, *Nanoscale*, 2014, **6**, 24-42.

68. J. Li, L. Z. Zhang, Y. J. Li and Y. Yu, *Nanoscale*, 2014, **6**, 167-171.

69. Y. Wu, H. Wang, Y. M. Sun, T. Xiao, W. G. Tu, X. Z. Yuan, G. M. Zeng, S. Z. Li and J. W. Chew, *Appl. Cata. B-Environ.*, 2018, **227**, 530-540.

70. C. T. Dinh, T. Burdyny, M. G. Kibria, A. Seifitokaldani, C. M. Gabardo, F. P. G. de Arquer, A. Kiani, J. P. Edwards, P. De Luna, O. S. Bushuyev, C. Q. Zou,

Materials Horizons Accepted Manuscript

R. Quintero-Bermudez, Y. J. Pang, D. Sinton and E. H. Sargent, *Science*, 2018, **360**, 783-787.

71. X. Sheng, Z. Liu, R. S. Zeng, L. P. Chen, X. J. Feng and L. Jiang, *J. Am. Chem. Soc.*, 2017, **139**, 12402-12405.

72. Z. Yin, H. Peng, X. Wei, H. Zhou, J. Gong, M. Huai, X. Li, G. Wang, J. Lu and L. Zhuang, *Energy Environ. Sci.*, 2019, 12, 2455-2462.

73. J. X. Liu, R. Li, X. Zu, X. C. Zhang, Y. F. Wang, Y. W. Wang and C. M. Fan, *Chem. Eng. J.*, 2019, **371**, 796-803.

74. K. Wang, Q. Li, B. S. Liu, B. Cheng, W. K. Ho and J. G. Yu, *Applied Catalysis B-Environmental*, 2015, **176**, 44-52.

75. S. Liu, M. Y. Zhao, Z. T. He, Y. Zhong, H. Ding and D. M. Chen, *Chin. J. Catal.*, 2019, **40**, 446-457.

76. F. Dong, Q. Y. Li, Y. J. Sun and W. K. Ho, *ACS Catal.*, 2014, **4**, 4341-4350.

77. T. Chen, Q. Hao, W. Yang, C. Xie, D. Chen, C. Ma, W. Yao and Y. Zhu, *Appl. Cata. B-Environ.*, 2018, **237**, 442-448.

78. H. Y. Deng, W. C. Hao and H. Z. Xu, *Chin. Phys. Lett.*, 2011, **28**, 4.

79. Q. Wang, W. Wang, L. L. Zhong, D. M. Liu, X. Z. Cao and F. Y. Cui, *Appl. Cata. B-Environ.*, 2018, **220**, 290-302.

80. X. Y. Huang, B. Li and H. Guo, *J. Alloy. Compd.*, 2017, **695**, 2773-2780.

81. H. Wang, D. Y. Yong, S. C. Chen, S. L. Jiang, X. D. Zhang, W. Shao, Q. Zhang, W. S. Yan, B. C. Pan and Y. Xie, *J. Am. Chem. Soc.*, 2018, **140**, 1760-1766.

82. X. Y. Kong, W. P. C. Lee, W. J. Ong, S. P. Chai and A. R. Mohamed, *Chemcatchem*, 2016, **8**, 3074-3081.

83. Y. Liu, Z. Jiang, X. Y. Zhang and P. K. Shen, *J. Mater. Chem. A*, 2018, **6**, 20037-20043.

84. J. Shang, W. Hao, X. Lv, T. Wang, X. Wang, Y. Du, S. Dou, T. Xie, D. Wang and J. Wang, *ACS Catal.*, 2014, **4**, 954-961.

85. S. Q. Jiang, L. Wang, W. C. Hao, W. X. Li, H. J. Xin, W. W. Wang and T. M. Wang, *J. Phys. Chem. C*, 2015, **119**, 14094-14101.

86. D.-L. Guan, C.-G. Niu, X.-J. Wen, H. Guo, C.-H. Deng and G.-M. Zeng, *J. Colloid Interface Sci.*, 2018, **512**, 272-281.

87. O. Mehraj, N. A. Mir, B. M. Pirzada and S. Sabir, *Appl. Surf. Sci.*, 2015, **332**, 419-429.

88. L. Hao, L. Kang, H. Huang, L. Ye, K. Han, S. Yang, H. Yu, M. Batmunkh, Y. Zhang and T. Ma, *Adv. Mater.*, 2019, **31**, 1900546.

89. L. Zhang, Y. Jia, G. Gao, X. Yan, N. Chen, J. Chen, M. T. Soo, B. Wood, D. Yang, A. Du and X. Yao, *Chem*, 2018, **4**, 285-297.

90. G. D. Sheng, A. Alsaedi, W. Shammakh, S. Monaquel, J. Sheng, X. K. Wang, H. Li and Y. Y. Huang, *Carbon*, 2016, **99**, 123-130.

91. G. D. Sheng, Y. N. Tang, W. S. Linghu, L. J. Wang, J. X. Li, H. Li, X. K. Wang and Y. Y. Huang, *Appl. Cata. B-Environ.*, 2016, **192**, 268-276.

92. C. W. Abney, R. T. Mayes, M. Piechowicz, Z. Lin, V. S. Bryantsev, G. M. Veith, S. Dai and W. Lin, *Energy Environ. Sci.*, 2016, **9**, 448-453.

93. D. Deng, X. Chen, L. Yu, X. Wu, Q. Liu, Y. Liu, H. Yang, H. Tian, Y. Hu, P.

Du, R. Si, J. Wang, X. Cui, H. Li, J. Xiao, T. Xu, J. Deng, F. Yang, P. N. Duchesne, P. Zhang, J. Zhou, L. Sun, J. Li, X. Pan and X. Bao, *Sci. Adv.*, 2015, **1**, 1500462.

94.   Q. F. Gong, P. Ding, M. Q. Xu, X. R. Zhu, M. Y. Wang, J. Deng, Q. Ma, N. Han, Y. Zhu, J. Lu, Z. X. Feng, Y. F. Li, W. Zhou and Y. G. Li, *Nat. Commun.*, 2019, **10**, 2807.

95.   E. Zhang, T. Wang, K. Yu, J. Liu, W. Chen, A. Li, H. Rong, R. Lin, S. Ji, X. Zhene, Y. Wang, L. Zheng, C. Chen, D. Wang, J. Zhang and Y. Li, *J. Am. Chem. Soc.*, 2019, **141**, 16569-16573.

96.   F. Zhou, L. M. Azofra, M. Ali, M. Kar, A. N. Simonov, C. McDonnell-Worth, C. Sun, X. Zhang and D. R. MacFarlane, *Energy Environ. Sci.*, 2017, **10**, 2516-2520.

97.   J. H. Montoya, C. Tsai, A. Vojvodic and J. K. Norskov, *ChemSusChem*, 2015, **8**, 2180-2186.